JOURNAL OF PROPULSION AND POWER
Vol. 24, No. 6, November–December 2008

Radical-Farm Ignition Processes in Two-Dimensional Supersonic Combustion

J. R. McGuire,* R. R. Boyce,† and N. R. Mudford‡
University of New South Wales, Australian Defence Force Academy, Canberra, New South Wales 2600, Australia

DOI: 10.2514/1.35562

A two-dimensional numerical study was performed of the ignition processes associated with the concept of radical farming for supersonic combustion. In a preliminary parametric study, a range of freestream conditions attainable in a hypersonic shock tunnel was investigated and mapped according to whether or not the behavior known as radical farming is present: a combustion-induced pressure rise in second or subsequent hot pockets rather than the first. Two such cases were analyzed in detail, both having mean conditions across the combustion-chamber entrance that would result in extremely long ignition lengths. The initiation, branching cycle, and heat release reactions in the combustion process become active in the radical farm, and H and OH radicals are produced. Their rate of production slows in the regions of flow expansion, but does not approach chemical freezing until toward the end of the localized expansion zones. Simultaneously, heat release elevates the local temperature. When the mixture flows through the shock at the second hot pocket, the elevated temperature and the presence of radicals enable the branching cycle and three-body recombination heat release reactions to accelerate, and significant pressure rise due to heat release is then able to occur. The extent to which this is completed in the second hot pocket depends on the inflow conditions.

I. Introduction

THE propulsion system most likely to be used for hypersonic airbreathing vehicles is the supersonic combustion ramjet, or scramjet. Scramjet research dates back to the late 1940s [1], and the reader is referred to Heiser and Pratt [2] and Curran and Murthy [3] for comprehensive historical and technical reviews of the research up to the end of the 20th century. However, a brief discussion of the key aspects of scramjets and supersonic combustion relevant to the present work is worthwhile here.

The basic principle of the scramjet is as follows. As seen from the frame of reference of the scramjet, the high-speed oncoming flow is compressed by shock waves in an inlet, resulting in air at higher pressure and temperature and a lower supersonic Mach number than the oncoming flow being delivered to the combustion chamber. Fuel, typically gaseous hydrogen or hydrocarbon, is injected into this oxidant stream and mixes with it. Under conditions favorable to ignition, combustion takes place. The attendant combustion heat release pressurizes the flow and lowers the combustion-chamber Mach number further. Thrust is generated by expanding the energized combustion products through an expanding nozzle at the flowpath exit.

At relatively low speed, typically less than Mach 8, the combustion heat release can lower the Mach number below unity, a condition known as thermal choking. This creates complex shock structures and large pockets of subsonic flow in the combustion chamber [2], and an extra flowpath section known as the isolator is then needed between the inlet and the combustion chamber to prevent the shock structure from unstarting the inlet [4]. A scramjet of this type operates as a ramjet at low supersonic speed and transitions to pure scramjet operation, defined subsequently, as the speed increases. Such scramjets are referred to as dual-mode ramjet/scramjets and were the focus of the bulk of scramjet research in the last quarter of the 20th century [5]. One of the key issues for this class of scramjet is the stability of the flame in the presence of the complex flow structures. Typically, recessed cavities or other such devices are used for flameholding purposes [6].

At higher flight speeds, the flow remains completely supersonic through the combustion chamber, apart from small regions of separated flow. Scramjets designed to operate in this mode are referred to as pure scramjets. Shock systems and combustion processes in pure scramjets are stable, and isolators are not required. However, the higher speeds at which they operate accentuate the need for the employment of mixing-enhancement techniques and reductions in ignition-delay lengths. Scramjets can thus be divided into two classes according to the flight speeds at which they are designed to operate. The present work is concerned with the second class of pure scramjet.

In his review paper, Ferri [7] points out that the flame in a pure scramjet is either a diffusion-controlled flame or a heat-conduction flame. In diffusion-controlled flames, nonpremixed air and fuel burn once they mix. For combustion to take place, the mixing must be achieved at the microscopic level. Such intimate mixing can only occur by molecular diffusion, although the rate of molecular diffusion can be accelerated by macroscopic mixing-enhancement techniques [5]. If the mixture temperature is high enough, then the combustion reaction rates are high and heat is released as fast as the mixing occurs. This is known as mixing-controlled combustion (for example, Wendt and Stalker [8]). On the other hand, if the mixture temperature is low, then the combustion reaction rates are low and the rate of heat release is governed by the chemistry and the combustion becomes reaction-rate-controlled (for example, Pulsonetti [9]). Heat-conduction flames are those where heat conduction from a combusting region, such as a pilot flame, into low-temperature premixed fuel–air raises the mixture temperature sufficiently for ignition to occur. This phenomenon can obviously also be used to accelerate the ignition of low-temperature diffusion-controlled flames.

A different way to accelerate ignition of low-temperature diffusion-controlled flames is to employ the oblique shock waves, which are almost always present in practical scramjet flowpaths, to raise the local static temperature of premixed fuel–air. If the shock elevates the reaction rates sufficiently that heat release occurs further

Received 8 November 2007; revision received 22 April 2008; accepted for publication 23 April 2008.

*Systems Engineer, School of Aerospace, Civil and Mechanical Engineering; currently Nova Defence, Brisbane, Australia.

†DSTO Chair for Hypersonics, Division of Mechanical Engineering; currently University of Queensland. Senior Member AIAA.

‡Senior Lecturer, School of Aerospace, Civil and Mechanical Engineering. Senior Member AIAA.

upstream than would be the case in the absence of the shock, then shock-induced ignition is said to have occurred [10]. If the reaction rates are greatly enhanced, the heat release occurs immediately behind the shock and couples to it to create an oblique detonation wave [11]. The former process, shock-induced ignition, is the focus of the present paper.

There is a particular class of scramjet that is of considerable interest in Australian hypersonics at present: the class in which fuel is injected from the compression ramps in the intake, enabling fuel–air mixing to occur upstream of the combustion chamber. A shock wave in the combustion chamber is then used to elevate the temperature and pressure of the mixture beyond the autoignition point, resulting in shock-induced combustion. Experimental shock-tunnel measurements by Gardner et al. [12] in a nominally 2-D version of such a scramjet employing discrete porthole hydrogen injection led to the concept of *radical farming* to describe the chemical kinetic processes that result in ignition and heat release. The flowpath that was investigated by Gardner et al. [12] is depicted schematically in Fig. 1. In this configuration, and in the absence of fuel injection, hot high-pressure pockets are formed in the flowfield between a system of shock and expansion waves propagating along the scramjet. Note that when fuel is injected, the flowfield will become three-dimensional, and if mixing is poor, the presence of a layer of cold fuel in the combustion chamber will further modify the flow structure. Figure 2 is an example of the results that pointed to the radical-farm concept. It shows the pressure distribution along the combustion-chamber lower wall for injection of hydrogen into both nitrogen and airflows. The former (the lower curve) shows the variation in surface pressure due to a shock/expansion system. The latter (the upper curve) shows the increase in pressure levels that resulted from combustion heat release. In this particular case, the mean conditions across the combustion-chamber entrance (the sharp expansion corner on the lower wetted surface in Fig. 1 and the origin in Fig. 2) were insufficient for rapid combustion (approximately 800 K and 80 kPa). On the other hand, the conditions in the first hot high-pressure pocket were approximately 1300 K and 200 kPa, sufficient for combustion to occur. The pressure plot of Fig. 2 shows that significant release of energy has only occurred once the flow reaches the second region of high temperature and pressure in the combustor.

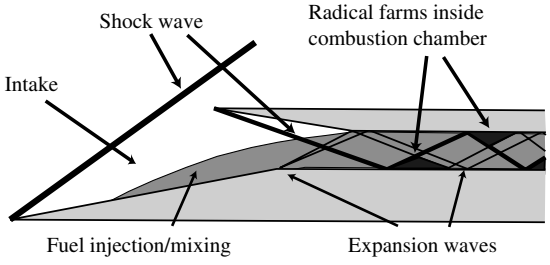

Fig. 1 Schematic of the scramjet model used by Gardner et al. [12]. The wetted surface consists of the intake compression surface and the combustion-chamber lower surface, separated by a sharp corner where the former ends and the latter begins. The upper wetted surface is the external cowl, responsible for the shock system in the combustion chamber.

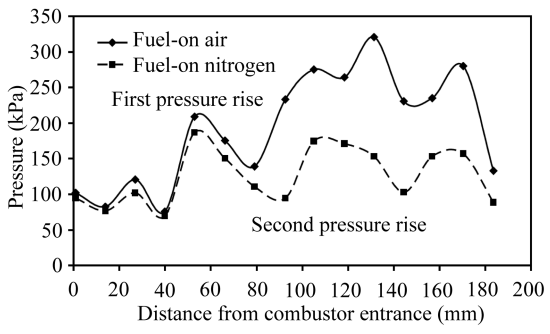

Fig. 2 Pressure profiles for reacting and nonreacting flow along the centerline of the model shown in Fig. 1.

Odam and Paull [13] conducted an experimental investigation of this effect, using fuel injection in a two-dimensional symmetric double-ramp intake followed by a straight-duct combustion chamber. They demonstrated that in such a configuration, combustion can be achieved even when the mean flow temperature is too low for this to occur without the shock/expansion system that propagates along the combustion chamber. Odam and Paull [13] then postulated the radical-farming concept: that in the first region of high temperature and pressure, dubbed the *radical farm*, the flow residence time is long enough to begin production of the chemical radicals such as H and OH that are necessary for ignition and heat release, but not long enough for the latter to occur. Before any significant heat release, the supersonic flow passes through an expansion wave in which radical production chemically freezes. Production recommences in hot pockets encountered further downstream, this time with sufficient concentration to allow heat release from combustion to occur. Depending on the flow conditions, several hot pockets may be necessary to complete this process.

To test this hypothesis, Odam and Paull [13] also conducted a one-dimensional theoretical analysis as follows. A hydrogen–air mixture initially at conditions typical of those in the radical farm was held at the radical-farm conditions for a time representative of the residence time in the farm, expanded to typical combustion-chamber mean flow conditions over a period representative of the residence time through such an expansion, held at those conditions for a further period of time, and then restored to the original conditions. Their analysis employed a modified form of the reaction scheme of Jachimowski [14]. The results showed that radicals were produced during the residence time in the radical farm, continued production in the expansion until a certain threshold temperature was reached, after which their concentration remained approximately constant, and then resumed production accompanied by combustion in the second hot pocket. Their conclusion was that the assumption of frozen radicals in the expansion was reasonable and that the accumulated residence time in the hot pockets was the primary factor that determined the occurrence of combustion.

Radical farming is an extremely significant concept, because it can be used to design scramjets that can operate with milder and hence more efficient intake compressions, such that the mean flow conditions entering the combustion chamber are too cold and/or too low in pressure for autoignition to occur. Knowledge of the precise way in which ignition occurs in such scramjets can therefore prove crucial for improving the efficiency and thus viability of scramjet technology. The present paper extends the analysis of Odam and Paull [13] to probe the coupling between the combustion kinetics and the flow structures in this class of scramjet. The paper presents a detailed numerical analysis of ignition processes in the radical-farm concept of supersonic combustion, using a generic two-dimensional flowpath.

II. Numerical Tools

The numerical tool employed here for the combustion flowfield simulations is the commercial computational fluid dynamics (CFD) code CFD++ [15]. CFD++ can solve both the steady or unsteady compressible and incompressible Navier–Stokes equations, including multispecies and finite-rate-chemistry modeling. Thermodynamic modeling of the flow is achieved by applying curve fits to thermodynamic data for each chemical species according to McBride et al. [16], whereas the species transport properties are specified according to the Sutherland law approximation. For turbulent Reynolds-averaged Navier–Stokes simulations, CFD++ has a range of turbulence models available, from one- to three-equation transport models. For all calculations in the present work, the two-equation realizable k-ε turbulence model was used, with a freestream turbulence level of 2% and a dimensional turbulence length scale of 0.01 m.

CFD++ is fundamentally an unstructured code, but handles Cartesian, structured curvilinear, and unstructured grids, including

hybrids. The calculations performed were double-precision and of second-order accuracy in both time and space. Concerning the spatial discretization, total-variation-diminishing polynomial interpolation with minmod limiting was used, whereas an implicit Runge–Kutta method was used for the time integration. Of particular importance is the fact that CFD++ has been subjected to extensive code-validation work. The reader is referred to various works in the literature for further information on the code and the code validation (for example, [15]).

The mesh consisted of 80 node points in the vertical direction and 798 points in the axial direction. In the vertical direction, the node points were clustered toward the wall to assist in resolving the boundary-layer flow, however, wall functions were also used for this purpose. The distance of the first node point from the wall at the inflow boundary is 0.05 mm, whereas in the combustor, this distance reduces to 0.028 mm. In the axial direction, the node points were equally spaced. The wall boundary condition assumed an isothermal wall at 293 K, to replicate a shock-tunnel flow.

Additional numerical tools were used to provide the inflow parameters for the simulations. These simulations were performed at conditions typically attainable in hypersonic shock-tunnel facilities, to be relevant to and guide experimental investigations of radical-farming processes [17]. The quasi-one-dimensional thermal equilibrium finite-rate-chemistry nozzle-expansion code STUBE [18] was employed with the reaction scheme of Lordi et al. [19] to simulate the flow through a Mach 6 shock-tunnel nozzle and into the test section for a variety of nozzle-reservoir total pressures and temperatures. The resulting freestream was chemically frozen and partially dissociated. The freestream conditions were then converted to conditions on the scramjet intake ramp using oblique shock theory, employing the software package HAP [2] and then completely mixed with the desired quantity of cold hydrogen fuel. The resulting conditions were then supplied as inflow boundary conditions for the CFD++ calculations reported here.

III. Hydrogen–Air Combustion Model

Hydrogen–air combustion involves a complex system of reactions involving initial reactants, intermediate species, and final products. A special class of intermediate species known as *free radicals* or *chain carriers* is particularly relevant to combustion reactions. These are formed when a covalent bond is broken, leaving a bonding electron on each of the resulting species. The unpaired electron makes radical species highly reactive. The relevant radicals for the hydrogen/air system are atomic oxygen (O), atomic hydrogen (H), and hydroxyl (OH).

The hydrogen–air chemistry model used for the present study was developed by Jachimowski [20], and the key reactions relevant to the discussions here are given in Table 1. This model contains 13 species and 33 reactions. The combustion process can be divided into the *ignition process* (consisting of the *initiation reaction* followed by the *branching cycle*) and the *heat release process*. In Table 1, reaction 1 and, initially, reaction 10 in the reverse direction are the initiation reactions for this model and result in the production of radicals.

Table 1 Jachimowski [20] finite-rate-chemistry model used for combustion calculations

Species number	Key reactions[a]
1	$H_2 + O_2 \rightleftarrows OH + OH$
2	$H + O_2 \rightleftarrows OH + O$
3	$O + H_2 \rightleftarrows OH + H$
4	$OH + H_2 \rightleftarrows H_2O + H$
6	$H + OH + M \rightleftarrows H_2O + M$
7	$H + H + M \rightleftarrows H_2 + M$
8	$H + O + M \rightleftarrows OH + M$
9	$H + O_2 + M \rightleftarrows HO_2 + M$
10	$HO_2 + H \rightleftarrows H_2 + O_2$
11	$HO_2 + H \rightleftarrows OH + OH$
20	$O + O + M \rightleftarrows O_2 + M$

[a]M represents the third bodies required for certain reactions.

Reactions 2, 3, and 4 together increase the number of radicals and are known as the branching cycle. These reactions are not associated with significant heat release, but are vital to the combustion process, because it is not until sufficient concentrations of chain carriers are present that heat release reactions accelerate. Reactions such as reaction 9, on the other hand, remove radicals from the system and are called *termination reactions*. For example, reaction 9 replaces the reactive radical H with the relatively nonreactive HO_2 molecule. Reactions 6, 7, 8, and 20 are the three-body reactions responsible for the majority of the combustion heat release. Because they are three-body reactions, they depend on the concentration of radicals being high for significant heat release to occur and thus depend on the branching cycle. They are thus also highly sensitive to pressure, whereas the two-body branching cycle reactions are more sensitive to temperature. In summary, the temperature-sensitive ignition process depends on two-body reactions that produce radicals, whereas the pressure-sensitive heat release process depends on the ignition process to produce the necessary radicals and then on the three-body reactions that recombine the radicals and produce H_2O. A useful definition of ignition for H_2–air combustion is that it occurs when the concentration of the H radical reaches a maximum (after which the recombination reactions quickly consume it) [21]. The temperature- and pressure-dependent finite rates at which the various steps in the combustion process occur are critically important in the context of supersonic combustion flowfields. The investigation of this in the context of the shock and expansion systems typically present in scramjet flowpaths is the focus of the studies presented in this paper.

Hydrogen–air combustion in enclosed vessels can be described in terms of boundaries in temperature–pressure space between explosive and nonexplosive behavior. Explosive behavior occurs when the rate of the branching reactions exceeds the rate of the termination reactions, which causes the concentration of radicals to increase and then rapid chemical reaction (ignition) and heat release to occur. When the termination reactions dominate, ignition does not occur. The *net branching factor* φ is defined [22] as the rate of branching reactions minus the rate of the termination reaction. The actual rates used in the net branching factor are those of the net production of the H radical. The rate-determining reaction in the branching cycle employed here is typically reaction 2 [23], and because the net stoichiometric mole number for H in the branching cycle is 2, the net branching factor is given by

$$\varphi = 2k_{(R2)}[H][O_2] - k_{(R9)}[H][O_2][M] \tag{1}$$

where the factor of 2 shown is the net stoichiometric mole number for H in the branching cycle. Rapid reaction, ignition, and heat release requires $\varphi > 0$. At $\varphi = 0$, Eq. (1) can be solved to give the *crossover temperature* T_c. Bearing in mind the simplification of the combustion reaction dependencies assumed in the definition of φ, the crossover temperature is a guide to the temperature above which rapid reactions in a scramjet combustion flow will occur. This will be used to assist the analysis presented later in this paper.

IV. Mesh Sensitivity Study

Details of the specific geometry considered in the present work are shown in Fig. 3. The main intake-ramp angle is 9 deg, the angle of the internal compression surface formed by the external cowl is 3 deg to the horizontal, the combustion chamber is 10.0 mm high, and the overall length is 445.0 mm. To generate supersonic combustion flows in which radical-farming phenomena are present, a premixed

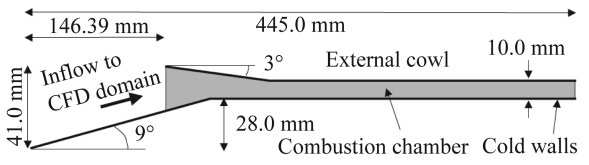

Fig. 3 Generic scramjet model used for the radical-farm investigations. The shaded region is the computational domain employed here.

H_2–air mixture determined using the numerical tools described earlier (STUBE and HAP) has been used as an inflow to the computational domain shown as the shaded region in the figure. A reduced computational domain was used for the calculations, in which the main intake ramp begins at the same streamwise location as the cowl. The inflow is set parallel to the intake ramp. Because of the reduced intake length simulated, the boundary layer will not be as developed as it would for a full ramp simulation. This does not alter the key phenomena or the conclusions resulting from the simulations.

A mesh sensitivity study was conducted to check the accuracy of the results obtained for both the parametric study and the subsequent more detailed analysis. A coarser mesh consisting of 60 node points in the vertical direction and 598 points in the axial direction was examined, along with a finer mesh consisting of 120 points in the vertical direction and 1198 points in the axial direction. Node points in the axial direction were spaced equally for each mesh, whereas the same distribution function was used for the points in the vertical direction. For each mesh, the same value for the first cell height at the wall was used. The freestream conditions used for each mesh in the sensitivity study were those of test case A and are given later in Sec. VI.

In Figs. 4 and 5, the pressure profiles along the lower surface of the model for frozen-chemistry calculations on each mesh are compared, along with the same profiles for a finite-rate-chemistry calculation. The pressure profiles for the frozen-chemistry calculation are almost identical, indicating that these solutions are mesh-independent. The profiles for the finite rate calculations, however, indicate slight differences in the solutions obtained on each mesh. Apart from the first hot pocket, where the peak pressure level in this region depends on the mesh, the remainder of the flow displays an almost identical level of pressure across each shock and expansion wave. The major difference lies in the location of the shock waves in the combustor, where the solution on the standard mesh shows that the shocks are displaced slightly from their corresponding location on the coarse and fine meshes. The conclusions drawn from this study are, however, thought to be unaffected by these differences.

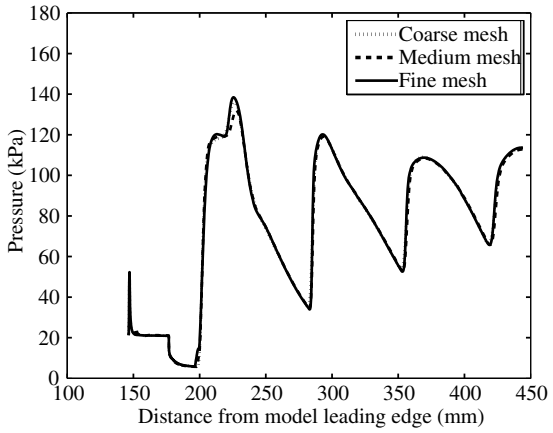

Fig. 4 Pressure profiles for the coarse, medium, and fine meshes for nonreacting flow.

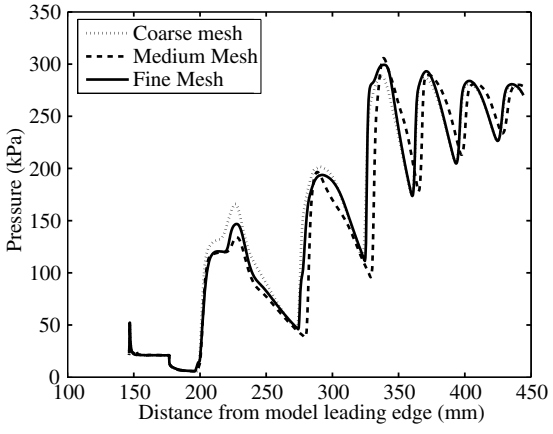

Fig. 5 Pressure profiles for the coarse, medium, and fine meshes for reacting flow.

V. Preliminary Parametric Study

A preliminary parametric study was performed for the flow through the generic scramjet model depicted in Fig. 3. The conditions examined are shown in Table 2. An equivalence ratio ϕ of 0.5 was used for all calculations. For each test condition, both reacting and nonreacting calculations were performed. Nonreacting flows were realized by specifying frozen chemistry for the simulations. Sample results comparing the reacting and nonreacting pressure profiles along the combustion-chamber lower wall are shown in Figs. 6–8, along with a sample frozen-chemistry pressure-contour plot that depicts the flow structures in the combustor. Based on the comparison of pressure profiles, each flow is classified here according to the following definitions:

1) In *noncombusting flow*, the combustion-induced pressure rise is less than 10% at the flow domain exit.

2) In *radical-farming flow*, the combustion-induced pressure rise is less than 10% in the first hot pocket, but greater than 10% at the flow domain exit.

3) In *combusting flow*, the combustion-induced pressure rise is greater than 10% in the first hot pocket.

Certain general features in the pressure distributions deserve highlighting. First, the steadily growing mean about which noncombusting pressure oscillates is due to boundary-layer growth. Second, the amplitude of the oscillations steadily decays, due to the smearing effect of the boundary layer on the shock/expansion system footprint. Third, the double-peak feature on the first hot-pocket pressure profile is a result of the weak shock from the intake-ramp leading edge reflecting from the cowl and returning to the lower wall. Finally, the transition due to combustion heat release from preignition profiles to post-heat-release profiles can be seen in the figure. For the radical-farm case, this occurs approximately over the length of the second hot pocket, after which the pressure profile behaves as for the frozen case, but at higher levels. This indicates that combustion has been more or less completed by the beginning of the third hot pocket. For the fully combusting case, this has occurred much more rapidly in the first hot pocket. Note that in the radical-farming case, the mean combustion-induced pressure attained toward the downstream end of the combustor is significantly greater than in the combusting case. This is due to the lower initial temperature in the former case, which has resulted in greater combustion efficiency than in the latter. Note also that hot pockets are

Table 2 Range of conditions examined in the parametric study

	T_o, K			
	2500	3000	4000	5000
P_o, MPa				
	2.63 MJ/kg	3.24 MJ/kg	4.76 MJ/kg	6.90 MJ/kg
20	2110 m/s	2329 m/s	2809 m/s	3304 m/s
	20.3 kPa	20.1 kPa	20.4 kPa	21.8 kPa
	334 K	404 K	603 K	916 K
16	2.63 MJ/kg	3.24 MJ/kg	4.80 MJ/kg	7.02 MJ/kg
	2119 m/s	2332 m/s	2819 m/s	3308 m/s
	16.4 kPa	15.9 kPa	16.3 kPa	17.5 kPa
	335 K	404 K	609 K	924 K
10	2.64 MJ/kg	3.25 MJ/kg	4.90 MJ/kg	7.28 MJ/kg
	2118 m/s	2335 m/s	2835 m/s	3313 m/s
	10.2 kPa	10.1 kPa	10.3 kPa	11 kPa
	335 K	404 K	617 K	929 K
6	2.64 MJ/kg	3.27 MJ/kg	5.03 MJ/kg	7.57 MJ/kg
	2113 m/s	2336 m/s	2836 m/s	3296 m/s
	6.1 kPa	6 kPa	6.2 kPa	6.5 kPa
	335 K	405 K	626 K	909 K

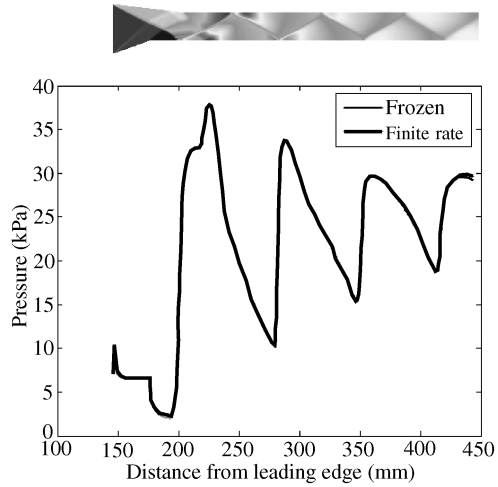

Fig. 6 Pressure profiles for a noncombusting flow; total pressure is 6 MPa and total temperature is 2500 K.

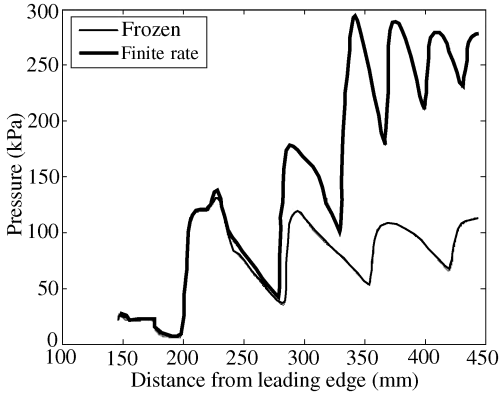

Fig. 7 Pressure profiles for a radical-farming flow; total pressure is 20 MPa, total temperature is 3000 K.

also located along the upper wall and radical farming or fully combusting behavior, depending on the inlet conditions, can also be observed there. For the purposes of this paper, only the flow near the lower surface is analyzed.

The results of the classification of the flows as combusting, noncombusting, and radical-farming flows are presented in Fig. 9. The radical-farming flows appear in a band between noncombusting and combusting flows. The rate of transition between the classifications can be seen from the figure to be more sensitive to changes in total temperature than to changes in total freestream pressure. This can be explained by the greater temperature sensitivity

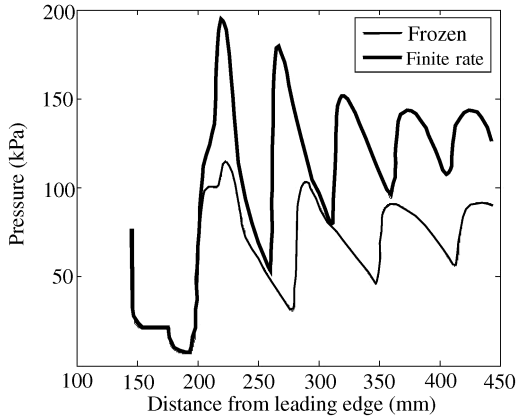

Fig. 8 Pressure profiles for a combusting flow; total pressure is 20 MPa, total temperature is 5000 K.

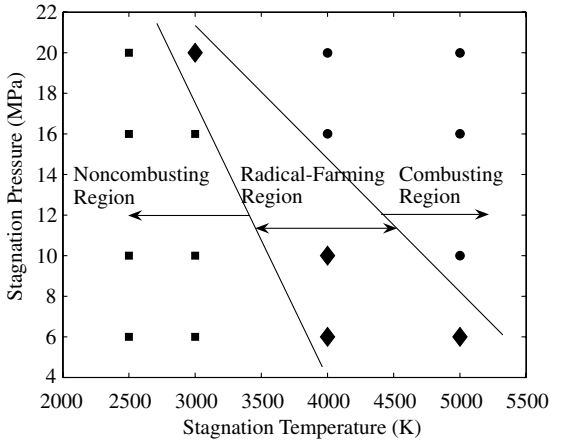

Fig. 9 Limits for combustion and radical farming in terms of stagnation temperature and pressure. Squares represent noncombusting flows, circles represent combusting flows, and diamonds represent flows that exhibit a radical-farm effect.

of the initiation reactions, whereas the pressure of the flow has more of an effect on the rate of heat release (in other words, the distance over which the heat release occurs).

VI. Detailed Analysis of Radical-Farm Ignition Processes

Using the preceding parametric study as a guide, two flowfields that would appear to give almost identical radical-farm ignition behavior have been generated and analyzed in detail. The two cases in fact turn out to have important differences in the path to ignition and heat release. The analysis and comparison is presented next for the combustion process along a streamline just above the lower wall and provides insight into the behavior of supersonic combustion in this class of scramjet.

Table 3 provides the inflow conditions for the two cases, which are labeled A and B. Both correspond to a flight Mach number, based on the total enthalpy, of approximately 8.0. The only difference between them is the local static temperature: 400 K for case A and 450 K for case B.

The pressure profiles for a streamline passing through the radical farm and hot pockets just above the wall for both combusting (reactions switched on) and noncombusting (reactions switched off) flows are shown for the two cases in Figs. 10 and 11. Also shown in the figures are pressure contours for both the combusting and noncombusting (reactions switched off) flows. These contour maps can be compared with the pressure profiles and clearly show the shock and expansion wave structures in the flowpath. It is important to note that in these simulations, there are no separated flow regions anywhere, such as can occur due to shock-induced boundary-layer separation. Such a flow feature would provide a hot subsonic region with long flow residence times that would significantly reduce ignition lengths and modify the phenomena being examined here. The pressure profiles exhibit the radical-farming appearance discussed earlier in this paper: rather than combustion-induced

Table 3 Inlet conditions for detailed analysis cases

	Case A	Case B
Pressure, kPa	20.1	20.1
Temperature, K	400	450
u velocity, m/s	2412	2412
v velocity, m/s	382	382
Global equivalence ratio ϕ	0.5	0.5
Mass fractions		
H_2	0.014	0.014
O_2	0.2297	0.2297
N_2	0.7559	0.7559

pressure rise occurring at the first hot pocket, which begins in these cases at approximately 200 mm from the virtual leading edge of the intake ramp, the pressure rise is delayed until the next hot pocket, which begins approximately 290 mm from the leading edge. A strong expansion, indicated by a significant decrease in pressure, sits between the first and second hot pockets. The question to be answered here is whether radicals are generated in the first hot pocket from initiation and branching cycle reactions, chemically frozen in the subsequent expansion, and then available for the three-body recombination reactions to proceed and release heat in the second hot pocket.

Figures 12 and 13 compare the static temperature along the streamlines of Figs. 10 and 11 for both cases and for reacting and nonreacting flows. In both cases, the nonreacting distributions display strong temperature decreases in the expansion between the first two hot pockets. On the other hand, the reacting distributions are fundamentally different for the two cases. In case A, the temperature decreases in the expansion, but remains slightly higher than the nonreacting version. In case B, there is a significant temperature *increase* that begins in the first hot pocket and continues for a large part of the expansion. Clearly, the reactions are proceeding at sufficiently different rates between cases A and B such that in the latter case, some heat release activity has occurred in the first hot pocket. The heat release is, however, insufficient to result in a pressure rise at the first hot pocket.

Figures 14–17 provide information on the production and consumption of the radicals H and OH along the streamline of interest, for cases A and B and for both nonreacting and reacting flows. Figures 16 and 17 also repeat the pressure distributions for all cases, from which the radicals can be correlated with the location of each hot pocket. Consider first the lower-temperature case, case A. From the pressure distribution, the first hot pocket begins approximately 205 mm from the leading edge, and the expansion system arrives at approximately 225 mm. The second hot pocket begins at approximately 290 mm. Radicals make their appearance toward the end of the *first* hot pocket, at 220 mm, and *increase* in abundance throughout the expansion before plateauing upstream of the second hot pocket, at approximately 270 mm. There is negligible pressure rise due to chemistry over this region and only a small increment in temperature (Fig. 12). This is an indicator that despite the chemical activity that is producing H and OH over this region, the branching cycle and the three-body recombination heat release reactions are not yet significantly active. This is confirmed with the variation of the reaction rates for the initiation reaction R1 (Fig. 18),

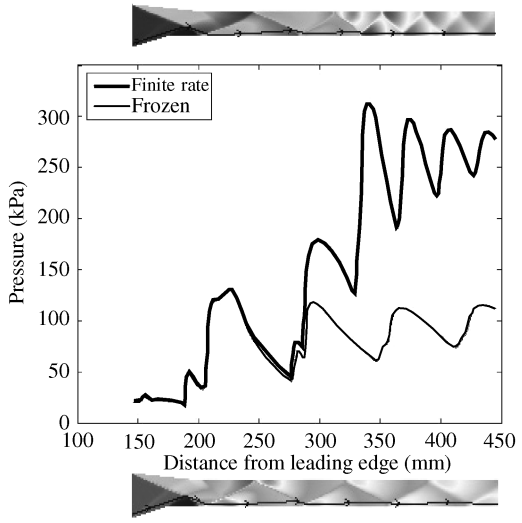

Fig. 10 Pressure profiles for test case A for combusting and noncombusting flows. Also shown are the pressure contours for the combusting and noncombusting flows above and below the plot, respectively.

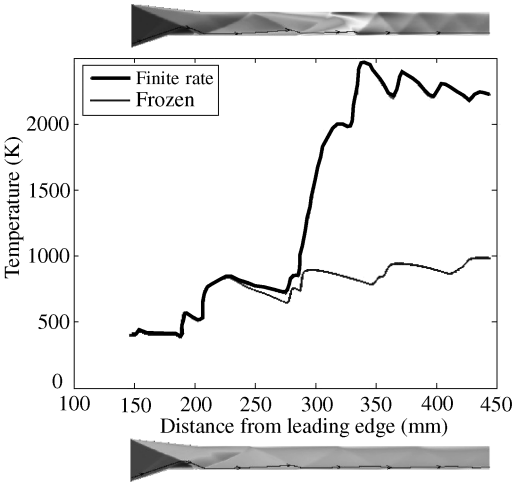

Fig. 12 Temperature profiles for test case A for combusting and noncombusting flows. Also shown are the temperature contours for the combusting and noncombusting flows above and below the plot, respectively.

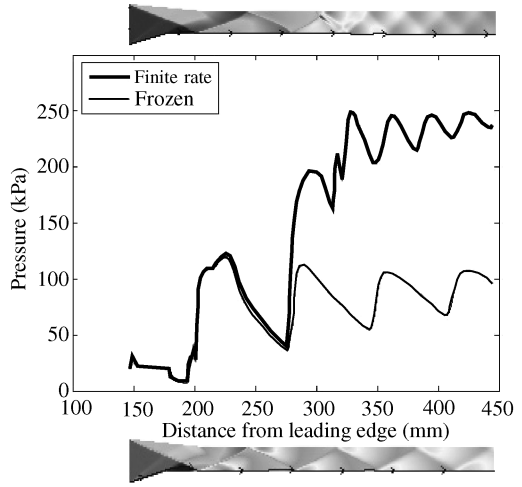

Fig. 11 Pressure profiles for test case B for combusting and noncombusting flows. Also shown are the pressure contours for the combusting and noncombusting flows above and below the plot, respectively.

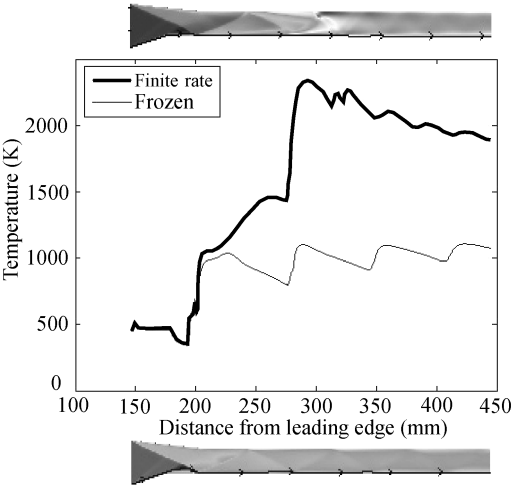

Fig. 13 Temperature profiles for test case B for combusting and noncombusting flows. Also shown are the temperature contours for the combusting and noncombusting flows above and below the plot, respectively.

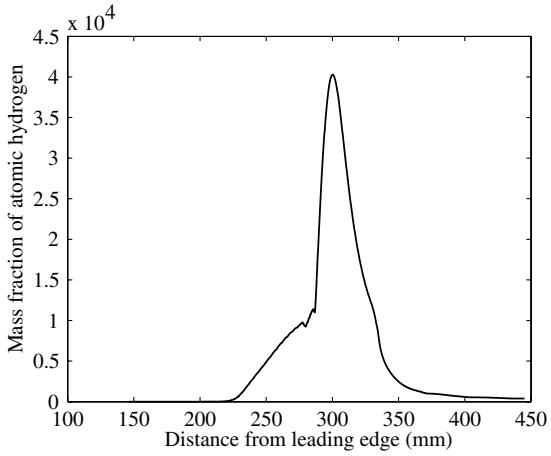

Fig. 14 Concentration and mass fraction profiles of atomic hydrogen (H) for the combusting flows of test case A.

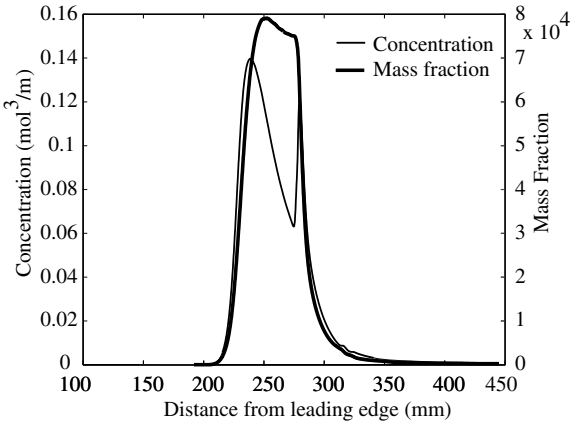

Fig. 15 Concentration and mass fraction profiles of atomic hydrogen (H) for the combusting flows of test case B.

one of the branching cycle reactions R3 (Fig. 19), one of the three-body recombination reactions R6 (Fig. 20), and the crossover temperature along the streamline (Fig. 21); compared with the second hot pocket, reaction rates are very low upstream of the second hot pocket. The local temperature is significantly *less* than the levels required for the branching cycle to be active and the mixture to become explosive. However, radicals *are* being produced in the first hot pocket. Consider Figs. 22–25, which show bar charts that provide the net reaction rate for each reaction in the system at the points along the streamline, indicated by black dots in Fig. 16. At 190 mm, just at

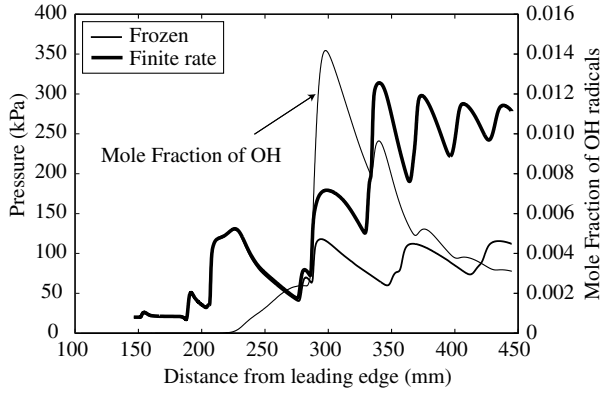

Fig. 16 Comparison of finite rate and frozen pressure profiles and the profile of mole fraction of OH radicals along the streamline for case A. The dots show locations at which reaction rates will be probed and discussed in the text.

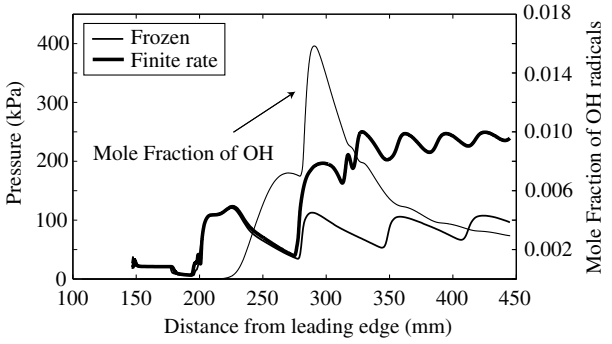

Fig. 17 Comparison of finite rate and frozen pressure profiles and the profile of mole fraction of OH radicals along the streamline for case B.

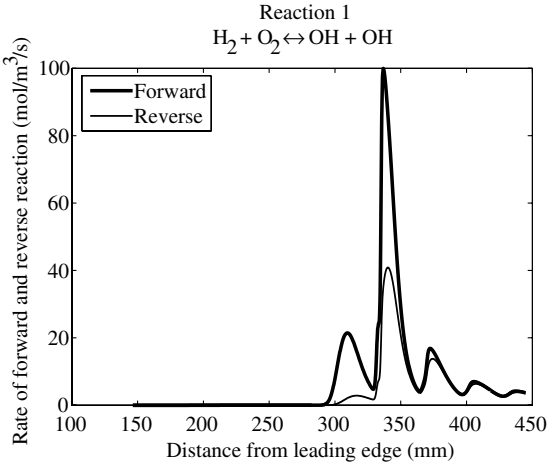

Fig. 18 Forward and reverse rates for the initiation reaction 1 along the streamline for case A.

the edge of the cowl shock but upstream of the first hot pocket, the initiation reaction R1 is dominant at *very* low rates. This is enough to enable the branching cycle to become active, and reaction R3 dominates the system behind the cowl shock at 202 mm, again at very low rates. Just inside the first hot pocket at 210 mm, the branching cycle reactions continue to dominate and are now 8 orders of magnitude faster than upstream of the first hot pocket. These reactions continue to accelerate through that hot pocket and into the expansion, such that inside the expansion at 251 mm, they are a further 3 orders of magnitude faster. The reaction rates achieved are sufficient for radical levels to have become appreciable, despite the rates still being insignificant compared with the second hot pocket. In summary, the first hot pocket has initiated the combustion process,

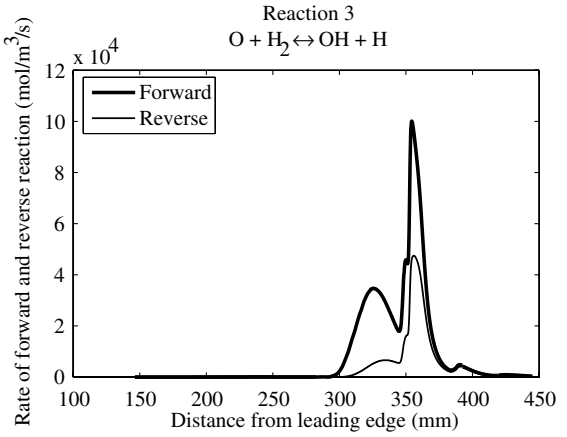

Fig. 19 Forward and reverse rates for branching cycle reaction 3 along the streamline for case A.

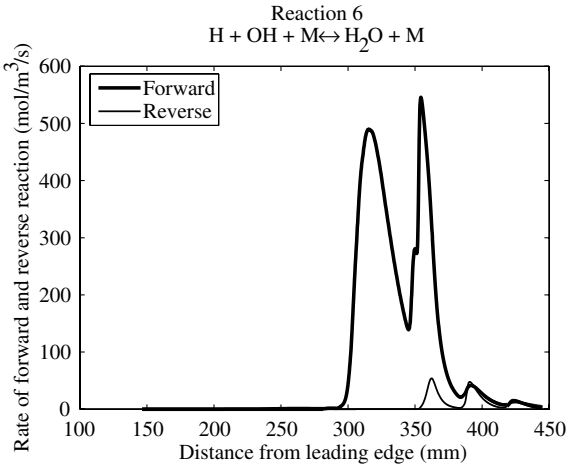

Fig. 20 Forward and reverse rates for the highly exothermic three-body recombination reaction 6 along the streamline for case A.

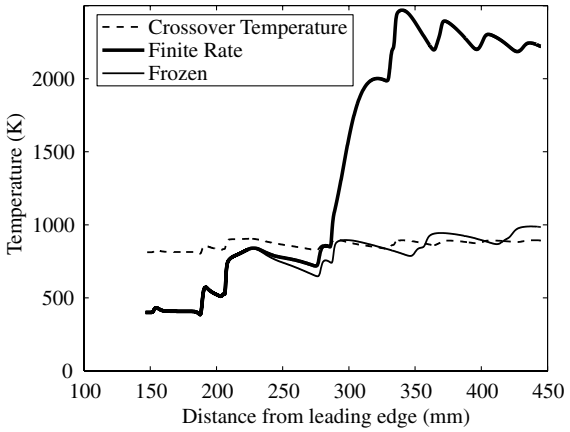

Fig. 21 Crossover temperature profile along the streamline for case A.

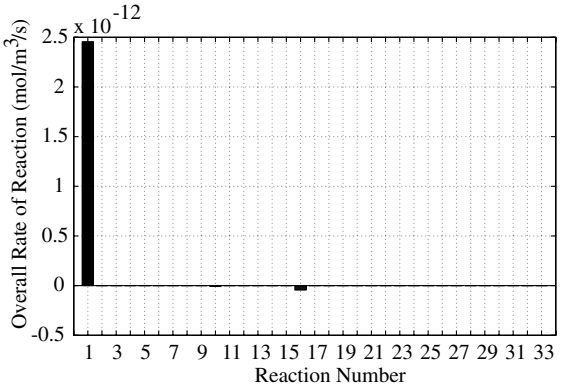

Fig. 22 Net reaction rates for each reaction just at the cowl shock, 190 mm, for case A.

radical production has begun, has *not* been quenched by the expansion, but has not occurred at a sufficient rate for ignition to be achieved by the first hot pocket alone. The first hot pocket is indeed a radical farm.

As soon as fluid enters the second hot pocket, the rates of the branching cycle reactions rapidly increase (Fig. 19), with the forward rates significantly higher than the reverse rates. Radical production accelerates (Figs. 14 and 16) such that the recombination heat release reactions also become very active (Fig. 20). Heat release raises the static temperature of the flow past the local crossover temperature; the mixture is now reactive. Over the passage through the second hot pocket, the recombination reactions begin to consume the radicals. The levels of H and OH have peaked in the second hot pocket, indicating that ignition has been achieved. The heat release begins

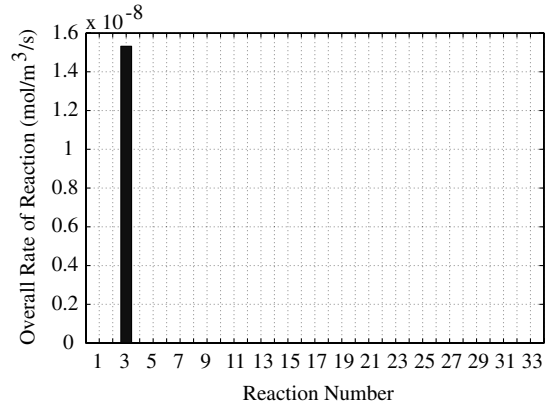

Fig. 23 Net reaction rates for each reaction just downstream of the cowl shock, 202 mm, for case A.

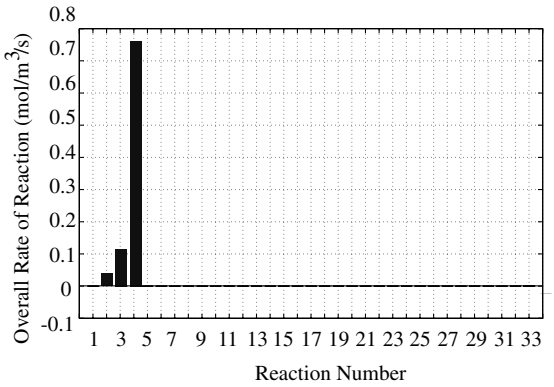

Fig. 24 Net reaction rates for each reaction just at the edge of the first hot pocket, 210 mm, for case A.

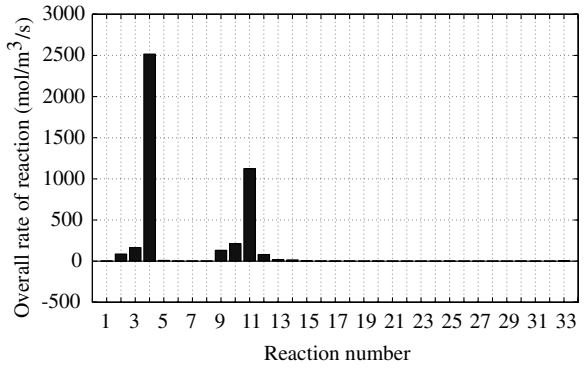

Fig. 25 Net reaction rates for each reaction downstream of the first hot pocket, 251 mm, for case A.

the process of increasing the pressure of the system (Fig. 16). However, the figures show that the radical consumption and heat release are not completed within the second hot pocket. The expansion after that hot pocket decreases the net rates of the branching cycle and heat release reactions, but not to zero; in other words, chemical activity still proceeds throughout that expansion, radicals continue to be consumed, and heat release continues to raise the temperature (Fig. 21). When the fluid reaches the third hot pocket at approximately 340 mm, the branching cycle accelerates once again and produces more radicals (this is most noticeable for OH), which the recombination reactions quickly begin consuming. The temperature now rises to its equilibrium level of approximately 2300 K, and the pressure rises to approximately 250 kPa, about which it oscillates throughout the remainder of the flow. The figures indicate that some chemical activity also occurs within the fourth and even fifth hot pockets, located at 380 and 410 mm, respectively, but this activity is very minor in comparison with the second and third hot pockets.

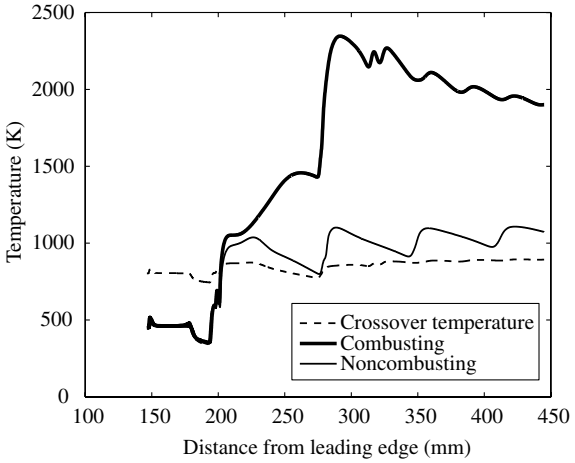

Fig. 26 Crossover temperature profile along the streamline for case B.

Consider now the higher-freestream-temperature case, case B. Referring again to Figs. 15, 17, and 26, we see immediately that the chemical behavior is different from case A. As Fig. 26 shows, the crossover temperature is exceeded at the beginning of the first hot pocket, even for the nonreacting flow, and so the mixture immediately becomes reactive. The reactions produce radicals very quickly, and significantly higher levels of H and OH are produced in the first hot pocket and into the subsequent expansion and peak midway through that expansion at approximately 250 mm. This peak does *not* represent ignition. Until this point, the temperature has steadily risen due to heat release reactions, but these, as well as the other reactions, are strongly influenced by the expansion, which is decreasing the pressure and thus the reaction rates. Despite minor removal of radicals by heat release reactions, seen in the downstream part of the expansion, the pressure rise due to heat release is so far very small. The net reaction rates become very small in this region, to the extent that heat release decreases so much that the local temperature is now able to begin decreasing as well (Fig. 26). The chemical activity is tending toward, but has not quite reached, frozen behavior due to the low pressures and hence low reaction rates. This is especially true for the pressure-sensitive three-body recombination reactions. However, the abundance of radicals is high. Compared with case A, the mole fraction of OH is more than double, but still not at the level reached at the ignition point in the case-A second hot pocket, whereas the mass fraction of H already exceeds the level at the case-A ignition point. As soon as the mixture reaches the second hot pocket, all reaction rates increase very quickly. The OH radical concentration increases to the level of case-A ignition and then decreases as the heat release reactions become active, whereas the H radical immediately begins the process of being consumed. The temperature rises quickly to the approximate 2300 K level of case A, whereas the pressure rises closer to its equilibrium levels than was the situation for case A. Note that these levels are slightly lower than for case A, a result of a decreased combustion efficiency due to the slightly higher inflow temperature. In contrast to case A, most of the heat release has thus been completed in the second hot pocket, due to the abundance of radicals upstream of this hot pocket. The third hot pocket does experience some chemical activity, but to a much lesser degree than case A.

To summarize the higher-temperature case, the first hot pocket is also a radical farm in which the mixture is reactive rather than nonreactive, to the extent that the branching cycle is playing an important role, not just the initiation reactions. Sufficient radicals have been produced that when the second hot pocket is reached, ignition and heat release occur rapidly and are mostly completed in that hot pocket.

The combustion presented here is shock-induced combustion, in which shock waves are deliberately used to ignite the flow (in other words, to raise the temperature and pressure to levels where ignition and heat release will occur rapidly). Herein lies a key advantage of radical farming. Consider the lower-temperature case, case A. The temperature and pressure in the radical farm are approximately 800 K and 120 kPa, respectively (Figs. 11 and 13). These conditions are, as previously discussed, nonreactive. The ignition-delay time correlation of Pergament [24], developed for standard atmosphere pressure stoichiometric hydrogen–air mixtures, is given by

$$\tau_{\text{id}} = 8 \times 10^{-3} \exp(9600/T)\mu s$$

At the approximate combustion-chamber entrance velocities of the work presented here (2400 m/s) and noting that these velocities do not vary significantly throughout the combustion chamber because they represent the bulk of the energy of the flow, the distance required for ignition would be on the order of 5000 mm. In the absence of the chemical reactions that have been observed here to occur in the radical farm, the conditions in the second hot pocket would represent no improvement in this situation. However, the reactions have not only generated radicals, but have also raised the temperature of the flow. Inspection of the reacting and nonreacting temperature profiles at the start of the second hot pocket for case A (Fig. 12) indicate that the postshock temperature in the second hot pocket is approximately 1200 K as a result of the radical farm. At this higher temperature, the distance required for ignition is now on the order of 100 mm according to the preceding correlation. Similarly for the higher-temperature case, case B, the radical-farm conditions are approximately 1000 K and 120 kPa, which would correspond to an ignition length on the order of 500 mm. The postshock temperature in the second hot pocket has risen to approximately 1500 K as a result of the radical-farm processes, corresponding to an ignition length on the order of 20 mm. These approximate values are of similar order to the ignition-delay lengths observed for both cases in the present work.

The comparison illustrates that the radical farm is serving two functions in the combustion process: it causes radicals to be generated that are needed for ignition, and by doing so it enables sufficient heat release to occur so that shock-induced combustion takes place at conditions that are favorable for rapid combustion. This is extremely important, especially because the mean conditions across the entrance to the combustion chamber are even milder than those in the radical farm. In other words, upstream injection/radical-farming/shock-induced combustion is a concept that can lead to fast rates of combustion heat release for flows that would normally have extremely slow rates.

VII. Conclusions

A two-dimensional numerical study was performed of the ignition processes associated with the concept of radical farming for supersonic combustion. In a preliminary parametric study, a range of freestream conditions attainable in a hypersonic shock tunnel was investigated and mapped according to whether or not the behavior known as radical farming is present: combustion-induced pressure rise in second or subsequent hot pockets rather than the first. Two such cases were analyzed in detail, both having mean conditions across the combustion-chamber entrance that would result in extremely long ignition lengths.

In the first, radicals were produced downstream of the cowl shock, upstream of the first hot pocket via the combustion initiation reaction. This enabled the branching cycle reactions to become active in the first hot pocket, accelerating the radical production. The chemical activity slowed in the expansion between the first and second hot pockets, but did not freeze. At the same time, low levels of heat release raised the temperature of the flow. When the mixture reached the second hot pocket, the existence of radicals in the flow and the elevated temperature enabled the branching cycle and recombination heat release reactions to become extremely active. Heat release accompanied by pressure rise occurred throughout the second hot pocket and into the next expansion. This was repeated to a lesser degree in the third and fourth hot pockets. The final equilibrium pressure level was partly reached in the second and almost fully reached in the third hot pocket.

In the second case, the higher inflow temperature led to sufficient chemical activity in the first hot pocket and through the subsequent

expansion that significant levels of radicals were produced and significant temperature rise occurred upstream of the second hot pocket. This led to rapid further OH radical production and then rapid radical consumption and heat release in the second hot pocket. The final equilibrium pressure rise was almost completely reached in the second hot pocket.

In summary, for this premixed two-dimensional configuration, the first hot pocket does indeed act as a radical farm. The initiation, branching cycle, and heat release reactions become active in the radical farm, and H and OH radicals are produced. Their rate of production slows in the regions of flow expansion, but does not approach chemical freezing until toward the end of the localized expansion zones. Simultaneously, heat release elevates the local temperature. When the mixture flows through the shock at the second hot pocket, the elevated temperature and the presence of radicals enables the branching cycle and three-body recombination heat release reactions to accelerate, and significant pressure rise due to heat release is then able to occur. The extent to which this is completed in the second hot pocket depends on the inflow conditions.

References

[1] Anderson, G. Y., McClinton, C. R., and Weidner, J. P., "Scramjet Performance," *Scramjet Propulsion*, edited by E. T. Curran, and S. N. B. Murthy, Progress in Astronautics and Aeronautics, Vol. 189, AIAA, Reston, VA, 2000.

[2] Heiser, W. H., and Pratt, D. T., *Hypersonic Airbreathing Propulsion*, edited by J. S. Przemieniecki, AIAA Education Series, AIAA, Washington, D.C., 1994.

[3] Curran, E. T., and Murthy, S. N. B. (eds.), *Scramjet Propulsion*, Progress in Astronautics and Aeronautics, Vol. 189, AIAA, Reston, VA, 2000.

[4] Van Wie, D., "Scramjet Inlets," *Scramjet Propulsion*, edited by E. T. Curran, and S. N. B. Murthy, Progress in Astronautics and Aeronautics, Vol. 189, AIAA, Reston, VA, 2000.

[5] Curran, E. T., Heiser, W. H., and Pratt, D. T., "Fluid Phenomena in Scramjet Combustion Systems," *Annual Review of Fluid Mechanics*, Vol. 28, 1996, pp. 323–360. doi:10.1146/annurev.fl.28.010196.001543

[6] Gruber, M. R., Baurle, R. A., Mathur, T., and Hsu, K. Y., "Fundamental Studies of Cavity-Based Flameholder Concepts for Supersonic Combustors," *Journal of Propulsion and Power*, Vol. 17, No. 1, 2001, pp. 146–153.

[7] Ferri, A., "Mixing-Controlled Supersonic Combustion," *Annual Review of Fluid Mechanics*, Vol. 5, 1973, pp. 301–338. doi:10.1146/annurev.fl.05.010173.001505

[8] Wendt, M. N., and Stalker, R. J., "Transverse and Parallel Injection of Hydrogen with Supersonic Combustion in a Shock Tunnel," *Shock Waves*, Vol. 6, No. 1, 1996, pp. 53–59. doi:10.1007/BF02511404

[9] Pulsonetti, M., "Scaling and Ignition Effects in Scramjets," *Proceedings of the 11th Australasian Fluid Mechanics Conference*, Vol. 1, Univ. of Tasmania, Hobart, Australia, 1993, pp. 431–434.

[10] Buttsworth, D. R., "Shock Induced Mixing and Combustion in Scramjets," Ph.D. Dissertation, Univ. of Queensland, Brisbane, Queensland, Australia, 1994.

[11] Pratt, D. T., Humphrey, J. W., and Glenn, D. E., "Morphology of Standing Oblique Detonation Waves," *Journal of Propulsion and Power*, Vol. 7, No. 5, 1991, pp. 837–845.

[12] Gardner, A. D., Paull, A., and McIntyre, T. J., "Upstream Porthole Injection in a 2-D Scramjet Model," *Shock Waves*, Vol. 11, No. 5, 2002, pp. 369–375. doi:10.1007/s001930200120

[13] Odam, J., and Paull, A., "Radical Farming in Scramjets," *Notes on Numerical Fluid Mechanics and Multidisciplinary Design*, edited by C. Tropea, S. Jakirlic, H.-J. Heinemann, H. Hnlinger, Vol. 96, Springer, Berlin, 2007.

[14] Jachimowski, C. J., "An Analysis of Combustion Studies in Shock Expansion Tunnels and Reflected Shock Tunnels," NASA TP-3224, 1992.

[15] Goldberg, U., Peroovian, O., Chakravarthy, S., and Sekar, B., "Validation of CFD + + Code Capability for Supersonic Combustor Flowfields," AIAA Paper 97-3271, 1997.

[16] McBride, B. J., Gordon, S., and Reno, M. A., "Coefficients for Calculating Thermodynamic and Transport Properties of Individual Species," NASA TM-4513, 1993.

[17] McGuire, J. R., Boyce, R. R., and Mudford, N. R., "Comparison of Computational and Experimental Studies on Shock Induced Ignition in Scramjets," AIAA Paper 2005-3394, 2005.

[18] Vardavas, I. M., "Modelling Reactive Gas Flows Within Shock Tunnels," *Australian Journal of Physics*, Vol. 37, No. 2, 1984, pp. 157–177.

[19] Lordi, J. A., Mates, R. E., and Moselle, J. R., "Computer Program for the Numerical Solution of Nonequilibrium Expansions of Reacting Gas Mixtures," NASA CR-472, 1965.

[20] Jachimowski, C. J., "An Analytical Study of the Hydrogen–Air Reaction Mechanism with Application to Scramjet Combustion," NASA TP-2791, 1988.

[21] Nicholls, J. A., "Stabilization of Gaseous Detonation Waves with Emphasis on the Ignition Delay Zone," Ph.D. Dissertation, Univ. of Michigan, Ann Arbor, MI, 1960.

[22] Lewis, B., and Von Elbe, G., "*Combustion, Flames, and Explosions of Gases*," Academic Press, New York, 1961.

[23] Sung, C. J., Li, J. G., Yu, G., and Law, C. K., "Chemical Kinetics and Self-Ignition in a Model Supersonic Hydrogen–Air Combustor," *AIAA Journal*, Vol. 37, No. 2, 1999, pp. 208–214.

[24] Pergament, H. S., "A Theoretical Analysis of Non-Equilibrium Hydrogen–Air Reactions in Flow Systems," AIAA—ASME Hypersonic Ramjet Conference, AIAA Paper 1963-113, 1963.

V. Yang
Editor-in-Chief